Generation of nondiffracting beams by spiral fields

José A. Ferrari, Eugenio Garbusi, and Erna M. Frins
Instituto de Física, Facultad de Ingeniería, J. Herrera y Reissig 565, 11300 Montevideo, Uruguay
(Received 16 December 2002; published 26 March 2003)

In this paper we demonstrate that spiral fields generate nondiffracting dark beams. A collimated laser beam incident on a compact disc, i.e., a commercial CD, was used as mask for the generation of spiral fields. We study theoretically and experimentally the intensity distribution near the axis of the optical system.

DOI: 10.1103/PhysRevE.67.036619 PACS number(s): 42.25.Fx, 42.30.Kq

I. INTRODUCTION

Optical beams of Bessel-type whose transverse intensity profile remains unchanged under free-space propagation are called nondiffracting beams [1–3]. Over the last decade, nondiffracting beams were intensively investigated for their unusual properties, such as self-imaging properties, wave front dislocations (optical vortices), robustness against obstacles in the propagation path, and their various applications, e.g., particle trapping, accurate path tracers, optical interconnections, and more recently applications in optical microlithography in which significant increase in depth of focus becomes especially useful for the fabrication of contact holes [4–7]. Nondiffracting beams can be generated using annular apertures placed in the back focal plane of a lens, by special conical optical elements known as axicons, holograms, diffractive elements, etc. [8–14].

It is worth noting that to actually generate a nondiffracting beam one should have a Bessel-beam of infinite extent, which in turn requires infinite energy. Thus, in real situations one obtains an approximation to a nondiffracting beam. Such beams are usually called *pseudo-non-diffracting* beams, which from the above discussion are characterized by an almost constant intensity profile over a finite region.

In this paper we demonstrate that electric fields with a spiral amplitude and/or phase modulation generate nondiffracting dark beams (more precisely, *pseudo-non-diffracting* beams). It is important to mention that in the literature the term ''spiral field'' refer to a field whose wave fronts are helical surfaces with axis along the propagation direction (z direction). In this context, a ''spiral phase plate'' means a plate with growing width proportional to the polar angle (see, e.g., Ref. [5], and the references therein). On the other hand, through the present paper the term ''spiral plate'' refers to a plate with a spiral groove engraved on its surface [i.e., a spiral on the (x,y) plane] and a ''spiral field'' will be the result of modulating a plane wave with such a mask (see the next section). We perform validation experiments using a compact disc, i.e., a commercial CD, as diffractive element for the generation of spiral fields and study the intensity distribution in the neighborhood of the axis of the system.

II. THEORY

Let us consider a semitransparent plate engraved with a spiral groove of N turns of pitch r_0 (i.e., r_0 is the radial distance between adjacent turns), with maximum and minimum radius $R_{\max}$ and $R_{\min}$, respectively (see Fig. 1). A cut of this plate through the center shows a periodic profile with period r_0. In principle, a periodic profile in the radial direction (r) can be mathematically described through an expression of the form

$$\sum_{n=-\infty}^{\infty} c_n \exp(2\pi i n r/r_0),$$

with c_n being complex constants. Now, making the substitution $2\pi r/r_0 \rightarrow 2\pi(r/r_0) - \theta$ we will obtain an expression for the spiral profile valid for all values of the polar angle θ.

Therefore, the general expression for the transmission factor $t(r,\theta)$ of this plate will be

$$t(r,\theta) = [H(r-R_{\min}) - H(r-R_{\max})] \sum_{n=-\infty}^{\infty} c_n \times \exp[2\pi i n(r/r_0) - in\theta]. \quad (1)$$

This transmission factor modulates phase and/or amplitude of the fields depending on the details of construction of the spiral plate, which in turn determinates the values of the constants c_n. $H(r)$ is the *step function* defined as $H(r)=1$ for $r>0$ and $H(r)=0$ elsewhere. Thus the factor $[H(r$

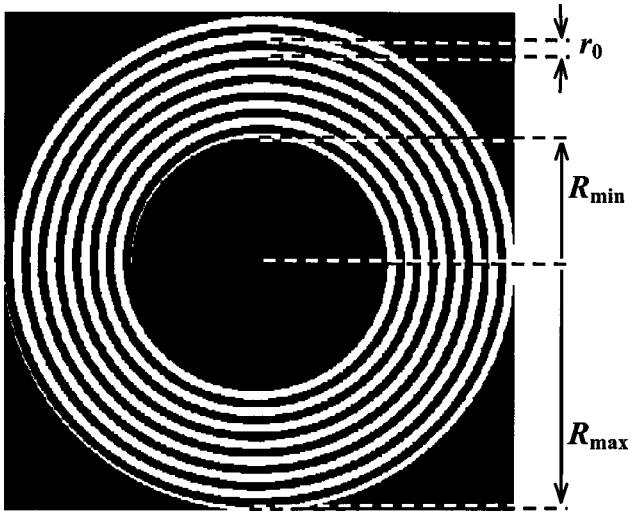

FIG. 1. Mask engraved with a spiral groove of N turns of pitch r_0 with maximum and minimum radius $R_{\max}$ and $R_{\min}$, respectively. In this figure $N=8$, but actually N could be arbitrarily large.

$-R_{\min})-H(r-R_{\max})]$ in Eq. (1) takes in account the fact that the transmission is zero outside of the region $R_{\min}\leqslant r \leqslant R_{\max}$.

Let us now consider a plane wave (wavelength λ) with electric field amplitude E_0 propagating along the z axis, orthogonal to the plane of the plate. The plate with transmission $t(r,\theta)$ is placed at $z=0$.

After the plate the diffracted field distribution will have two parts:

$$E(r',\theta',z)=E_{\text{aperture}}(r',\theta',z)+E_{\text{spiral}}(r',\theta',z), \quad (2)$$

where E_{aperture} is the field diffracted by a homogeneous annular aperture [i.e., the term with $n=0$ in Eq. (1)],

$$E_{\text{aperture}}(r',\theta',z)=\frac{E_0 c_0 \exp(i\pi r'^2/\lambda z)}{i\lambda z}\int_{R_{\min}}^{R_{\max}}\int_0^{2\pi}\exp(i\pi r^2/\lambda z) \times\exp[-i2\pi(rr'/\lambda z)\cos(\theta-\theta')]r\,d\theta\,dr, \quad (3)$$

and E_{spiral} is the diffracted field due to the terms with $n\neq 0$ in Eq. (1),

$$E_{\text{spiral}}(r',\theta',z)=\frac{E_0 \exp(i\pi r'^2/\lambda z)}{i\lambda z}\sum_{n=1}^{\infty}\int_{R_{\min}}^{R_{\max}}\int_0^{2\pi}\{c_n\exp[2\pi in(r/r_0)-in\theta]+c_{-n}\exp[-2\pi in(r/r_0)+in\theta]\} \times\exp(i\pi r^2/\lambda z)\exp[-i2\pi(rr'/\lambda z)\cos(\theta-\theta')]r\,d\theta\,dr. \quad (4)$$

The diffracted field due to an annular aperture—Eq. (3)—is well known, and a detailed discussion can be found in the literature [15]. The objective of the present paper focuses on the expression (4).

It is convenient to write

$$E_{\text{spiral}}(r',\theta',z)=\sum_{n=1}^{\infty}E_n(r',\theta',z),$$

with

$$E_n(r',\theta',z)=\frac{E_0 \exp(i\pi r'^2/\lambda z)}{i\lambda z}\int_{R_{\min}}^{R_{\max}}\int_0^{2\pi}\{c_n\exp[2\pi in(r/r_0)-in\theta]+c_{-n}\exp[-2\pi in(r/r_0)+in\theta]\} \times\exp(i\pi r^2/\lambda z)\exp[-i2\pi(rr'/\lambda z)\cos(\theta-\theta')]r\,d\theta\,dr. \quad (5)$$

Each of the partial fields E_n represents the diffracted field by the nth mode of the Fourier decomposition of the spiral groove. Performing the integration in the variable θ, results in

$$E_n(r',\theta',z)=\frac{E_0 \exp(i\pi r'^2/\lambda z)\pi i^{-n}}{i\lambda z}\left\{c_n\exp(-in\theta')\int_{R_{\min}}^{R_{\max}}\exp[i(\pi r^2/\lambda z+2\pi nr/r_0)] \times J_n(2\pi rr'/\lambda z)r\,dr+c_{-n}\exp(in\theta')\int_{R_{\min}}^{R_{\max}}\exp[i(\pi r^2/\lambda z-2\pi nr/r_0)]J_n(2\pi rr'/\lambda z)r\,dr\right\}, \quad (6)$$

where J_n is the Bessel function of first kind and order n.

This expression is still too complicated to obtain an exact analytical solution in closed form. To obtain an approximate solution, it is convenient to rewrite the above expression in terms of adimensional parameters.

We shall make the following substitutions:

$$r\to Rr, \quad r'\to\lambda r', \quad z\to Rz, \quad (7)$$

where $R=1$ cm and the *new* r, r' and z are now adimensional parameters. Also, let us define the adimensional parameters

$$a\equiv R/r_0, \quad b\equiv r_0/\lambda. \quad (8)$$

Using the above defined adimensional parameters, the expression (6) can be rewritten as

$$E_n(r',\theta',z)=\frac{E_0 ab\exp(i\pi r'^2/abz)\pi i^{-n}}{iz}\left\{c_n\exp(-in\theta')\int_{R_{\min}/R}^{R_{\max}/R}\exp[ia(\pi br^2/z+2\pi nr)]J_n(2\pi rr'/z)rdr\right.$$
$$\left.+c_{-n}\exp(in\theta')\int_{R_{\min}/R}^{R_{\max}/R}\exp[ia(\pi br^2/z-2\pi nr)]J_n(2\pi rr'/z)rdr\right\}. \quad (9)$$

Specifically, we shall consider a spiral with a large number of turns (e.g., $N\sim 10^4$ or even larger). Thus, r_0 will be of the order of microns and the parameter $a(=R/r_0\sim N)$ will be very large. For large values of a the integral (9) can be approximated as an asymptotic expansion in $a^{-k/2}$ being $k=1,2,...$, using the *method of the stationary phase* [16,17]. The two integrals appearing in Eq. (9) are of the general form

$$E_n(r',\theta',z)=\int_A^B f(r)\exp[ia\mu(r)]dr, \quad (10)$$

with $f(r)=J_n(2\pi rr'/z)r$ and $\mu(r)=\pi br^2/z\pm 2\pi nr$. Since $\mu''(r)=$const (with $\mu''\equiv d^2\mu/dr^2$), the first two terms in the asymptotic expansion are (see, e.g., Ref. [16] pp. 235–239)

$$E_n(r',\theta',z)=[\pi/2a\mu''(r_1)]^{1/2}\exp(i\pi/4)f(r_1)\times\exp[ia\mu(r_1)]+(1/ia)\{f(B)\times\exp[ia\mu(B)]/\mu'(B)-f(A)\times\exp[ia\mu(A)]/\mu'(A)\}+\cdots, \quad (11)$$

where μ' is the first derivative of μ and r_1 is the root of the equation $\mu'(r)=0$.

In the first integral in Eq. (9) we have $\mu(r)=\pi br^2/z+2\pi nr$, then the root of $\mu'(r)=0$ is $r_1=-nz/b$. Since this stationary point is not in the interval $[(R_{\min}/R),(R_{\max}/R)]$, the asymptotic expansion of this integral starts with the term in $1/a$. On the other hand, for the second integral of Eq. (9) we have $\mu(r)=\pi br^2/z-2\pi nr$, and thus $r_1=nz/b$. Since this stationary point is interior to the integration interval when $(R_{\min}/R)<r_1<(R_{\max}/R)$, the asymptotic expansion of the second integral starts with the term in $(1/a)^{1/2}$ for $(r_0/n\lambda)R_{\min}<z<(r_0/n\lambda)R_{\max}$. Therefore, to first order in $(1/a)^{1/2}$ only the contribution of the second integral is important.

From Eqs. (9)–(11), for $(r_0/n\lambda)R_{\min}<z<(r_0/n\lambda)R_{\max}$ we can write

$$E_n(r',\theta',z)\approx nE_0c_{-n}\pi i^{-(n+1)}\times\exp(i\pi/4)(az/4b)^{1/2}\exp(in\theta')\times\exp(-ia\pi n^2z/b)J_n(2\pi nr'/b)+\cdots, \quad (12)$$

where the terms of higher order have amplitudes smaller than the first order expression shown above by a factor $(1/a)^{1/2}$ at least. Thus, for large values of a (e.g., $a\sim 10^4$) higher order terms can be neglected.

Now, making the back-transformation to dimensional parameters

$$r'\to r'/\lambda, \quad z\to z/R \quad (13)$$

[being the *new* (r',z)-dimensional parameters] and recalling that $a\equiv R/r_0$, $b\equiv r_0/\lambda$, to first order we can rewrite Eq. (12) as

$$E_n(r',\theta',z)\simeq nE_0c_{-n}\pi i^{-(n+1)}\times\exp(i\pi/4)(z\lambda/4r_0^2)^{1/2}\exp(in\theta')\times\exp(-i\pi n^2z\lambda/r_0^2)J_n(2\pi nr'/r_0) \quad (14)$$

for

$$(r_0/n\lambda)R_{\min}<z<(r_0/n\lambda)R_{\max}. \quad (15)$$

The field is some orders of magnitude lower outside this region [the exact amplitude of the field depends on the value of $(1/a)^{1/2}$].

Expression (14) shows that the nth mode propagates without spreading (i.e., it is a nondiffracting beam) in the region $(r_0/n\lambda)R_{\min}<z<(r_0/n\lambda)R_{\max}$ and it is negligible outside this region. Thus, depending on the mode number (n) one may identify zones for each mode on the z axis. Lower order modes are located farther than higher ones, but it is clear that different modes may overlap. One can expect abrupt intensity changes at the frontiers of the modes due to different c_{-n} coefficients.

Since $J_n(0)=0$ for $n\neq 0$, the expression (14) describes a "dark" nondiffracting beam with zero field amplitude on the z axis. In general, the dominant terms in the Fourier series shown in Eq. (1) are the terms with $|n|\leqslant 1$. Thus, an estimation of the width of the bright annulus around the dark region centered on the z axis can be done by recalling that the first maximum of $J_1(2\pi r'/r_0)$ is for $2\pi r'/r_0\simeq 1.841$. Then, the bright annulus will have a radius $r'\sim 0.3r_0$. When n increases the first maximum of $J_n(2\pi nr'/r_0)$ does not necessarily translate towards larger values of r', but even for $n=10$ the radius of the beam will not exceed $0.2r_0$.

Note also that in general $(R_{\min}/nr_0)\gg 1$, so in the region of the z axis where the nondiffracting beam exists will be also $(z\lambda/r_0^2)^{1/2}\gg 1$. Therefore, from Eq. (14) it is clear that the intensity of the beam ($|E_n|^2$) in the neighborhood of the axis could be several orders of magnitude greater than the intensity ($|E_0|^2$) of the incident plane wave.

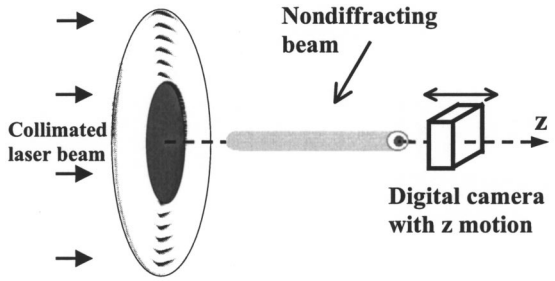

FIG. 2. Experimental setup. An expanded laser beam is incident on a semitransparent mask with a spiral groove. The intensity distribution of the diffracted field is acquired with a digital camera which has z motion.

III. EXPERIMENTAL RESULTS

As phase and amplitude mask we have used a commercial compact disc (CD). CD's have a thin layer of reflecting metal covered by a semi-transparent layer of plastic. In recordable CD's, in the interface plastic-metal there is an engraved (stamped, molded, or etched) spiral whose detailed structure depends on the fabrication process. The metal layer of a recordable CD can be easily separated from the plastic cover. This cover still retains some (amplitude and phase) spiral information on its surface, and therefore, it can be used as a semitransparent plate for the modulation of an incident plane wave.

The standard dimensions of commercial CD's are $R_{\min} \simeq 2.2 \pm 0.1$ cm and $R_{\max} \simeq 5.8 \pm 0.1$ cm. The value of the spiral pitch (r_0) is an important parameter in our physical model. The typical value mentioned in the literature [18] is $r_0 = 1.6\ \mu$m. In simple diffraction experiments performed on several of CD's using a narrow laser beam, it was possible to determine the actual distance between grooves. We found that for the CD used in our experiments the value of the pitch is $r_0 \simeq 1.5 \pm 0.1\ \mu$m.

A sketch of the setup to generate nondiffracting beams is shown in Fig. 2. An expanded laser beam ($\lambda = 0.532\ \mu$m) is incident on the plastic cover of a CD placed at $z = 0$. From the expression (15) we conclude that the mode $n = 1$ can exist for $6.2\ \text{cm} < z < 16.4\ \text{cm}$, the mode $n = 2$ for $3.1\ \text{cm} < z < 8.2\ \text{cm}$, the mode $n = 3$ for $2.1\ \text{cm} < z < 5.5\ \text{cm}$, and so on.

Figure 3 shows a lateral cut of the intensity distribution along the z axis. This image was acquired placing a sheet of black paper in a plane orthogonal to the CD through its axis. A very concentrated light beam is shown in the central region of the image along the z axis. Superposed to the raw image we have indicated with white characters and lines the regions where the different modes can exist.

The image shows that an intense narrow light beam extends from $z \simeq 2$ cm to $z \simeq 16$ cm without apparent broadening, which is in good agreement with the calculated maximum and minimum values of z for the modes from $n = 1$ to $n = 3$. The abrupt intensity change at $z \simeq 6$ cm coincides very well with the beginning of the zone where the mode $n = 1$ exists. In this image there are not abrupt intensity changes at the beginning nor the end of the zone for the mode $n = 2$.

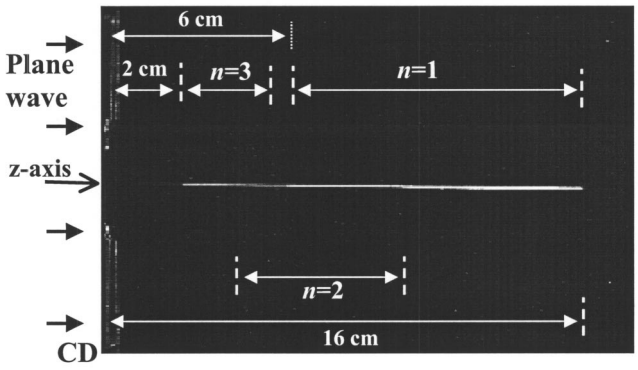

FIG. 3. Lateral cut of the intensity distribution along the z axis. A narrow light beam in the central region of the image along the z axis is shown. We superposed white characters and lines to indicate the regions where the different modes can exist.

Figures 4(a)–4(f) show the intensity distribution in a plane orthogonal to the z axis for different distances to the CD. The figures correspond to following distances: (a) $z = 3$ cm, (b) $z = 6$ cm, (c) $z = 7$ cm, (d) $z = 9$ cm, (e) $z = 12$ cm, and (f) $z = 14$ cm.

The images were acquired with a digital camera (244×753 pixels) without lens. The size of a pixel is $13.5\ \mu\text{m} \times 11.5\ \mu$m. In all images the light beam is concentrated essentially on the area of a pixel, and the light intensity decays rapidly in a couple of pixels around the central one. This is consistent with the order of magnitude of the beam radius

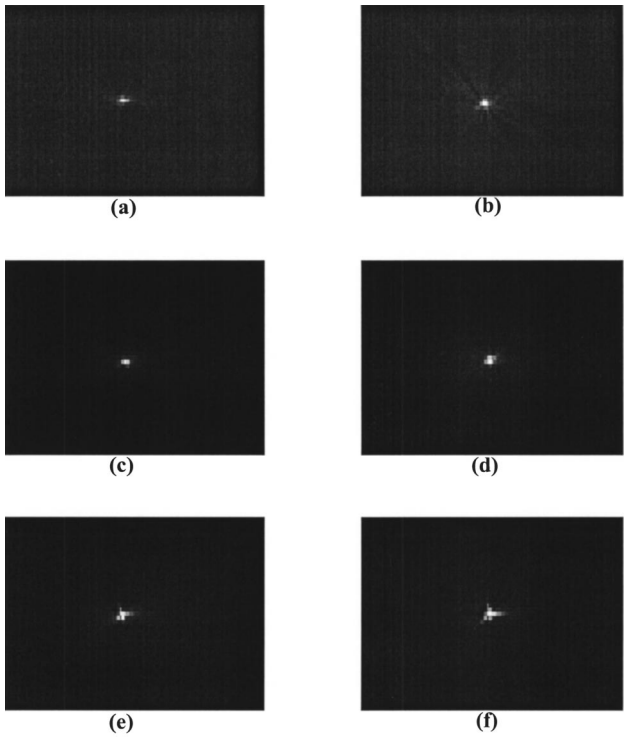

FIG. 4. Intensity distribution in a plane orthogonal to the z axis for different distances to the CD. The figures correspond to the distances (a) $z = 3$ cm, (b) $z = 6$ cm, (c) $z = 7$ cm, (d) $z = 9$ cm, (e) $z = 12$ cm, and (f) $z = 14$ cm.

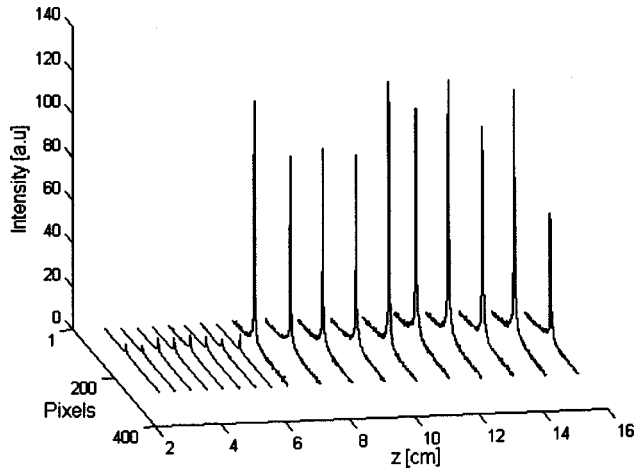

FIG. 5. Evolution of the nondiffracting beam along the z axis. Note the abrupt intensity change at $z \simeq 6$ cm that coincides with the beginning of the mode $n=1$.

calculated above. Evidently, since the pitch (r_0) of our spiral is very small, it is not possible to observe the dark region inside the bright annulus, because this would imply to resolve a fraction of micron ($\sim 0.3 r_0$).

Figure 5 shows the evolution of the nondiffracting beam profile along the z axis. Again this figure shows the abrupt intensity change at $z \simeq 6$ cm that coincides with the beginning of the mode $n=1$. In this figure it is not clear to see the growth of the light intensity as $z^{1/2}$—predicted by Eq. (14)—inside the region corresponding to a mode. Probably, this is due to mode superposition in the central region from $z \simeq 3$ cm to $z \simeq 8$ cm. We have no explanation for the intensity decrease at the end of mode $n=1$ around $z \simeq 16$ cm.

Figure 6 shows an opaque obstacle placed in front of the

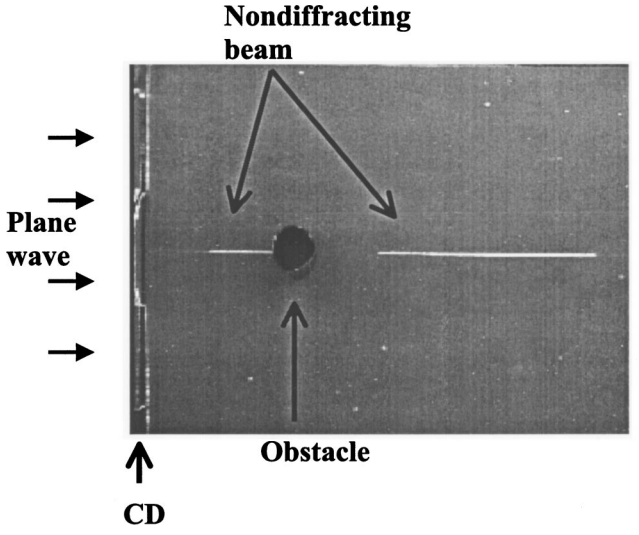

FIG. 6. Obstacle blocking the intense beam propagating along the axis. Some centimeters beyond the obstacle, the beam is self-reconstructed.

CD on the z axis, which blocks the intense beam propagating along the axis. It is shown that some centimeters beyond the obstacle, the beam is self-reconstructed. This self-reconstruction is a characteristic of the nondiffracting beams, which has been extensively studied in the literature [5,6].

IV. DISCUSSION AND CONCLUSIONS

In this paper we study the propagation of spiral fields. We decomposed the spiral field in harmonic components (i.e., ''modes''), and found that the nth component generates a Bessel beam $E_n \sim \exp(in\theta') J_n(2\pi n r'/r_0)$ that propagates along the z axis without broadening, i.e., the spiral field generate a dark nondiffracting beam whose radius is a fraction of the pitch (r_0) of the spiral. The proportion of the total energy associated to each mode depends on the Fourier coefficients c_{-n}. That is, it depends on the detailed structure of the mask used for generating the spiral field. In general, it is physically reasonably to expect that the dominant mode will be $n=1$, and that perhaps, some other modes for small values of n will be present.

Also, we demonstrated that each mode is located in a precise portion of the z axis given by the formula $(r_0/n\lambda)R_{\min} < z < (r_0/n\lambda)R_{\max}$, where $R_{\min}$ and $R_{\max}$ the minimum and maximum spiral radius, respectively. Our calculations are based on the *method of the stationary phase*, which applies when the parameter a ($=R/r_0$) is large.

In order to support our theoretical conclusions we performed some experiments using the plastic cover of a recordable compact disk (CD) as a mask to modulate an expanded laser beam. For a CD $a \sim 10^4$, thus the second order approximation to the diffracted field is 10^2 times smaller than the first order approximation used in our calculations. Therefore, the application of the *method of the stationary phase* to first order is absolutely justified.

Our experimental results are shown in the Figs. 3–6. The images acquired with a digital camera show a very narrow light beam (with lateral dimensions of the order of microns) propagating several centimeters without broadening along the disk axis. In the images it is clearly observed that the nondiffracting beam has an abrupt beginning and an abrupt end that coincides (with an accuracy of the order millimeters) with the theoretical values predicted for the modes $n=1$ and $n=3$. Also, we observed the characteristic self-reconstruction property of nondiffracting beams.

Evidently, since only a very little of the total energy of the input beam is diffracted by the plastic cover, its efficiency to generate high-order nondiffracting modes is not very high. A higher diffraction efficiency can be achieved by light reflection on an entire CD (i.e., without taking off the metal layer).

As a final remark, we have to mention that an extremely intense nondiffracting beam can be generated by reflection using sun light. In this case, the wavelength dependence of the expression $(r_0/n\lambda)R_{\min} < z < (r_0/n\lambda)R_{\max}$ can be easily observed. Also, using a digital versatile disk (DVD), for which typically $r_0 \sim 0.7\ \mu$m, the zone-pitch dependence for the different modes can be verified.

[1] J. Durnin, J. Opt. Soc. Am. A **4**, 651 (1987).
[2] J. Durnin, J. J. Miceli, Jr., and J. H. Eberly, Phys. Rev. Lett. **58**, 1499 (1987).
[3] G. Indebetouw, J. Opt. Soc. Am. A **6**, 150 (1989).
[4] M. Erdélyi, Z. L. Horváth, G. Szabó, Zs. Bor, F. K. Tittela, J. R. Cavallaro, and M. C. Smayling, J. Vac. Sci. Technol. B **15**, 287 (1997).
[5] Z. Bouchal, Opt. Commun. **210**, 155 (2002).
[6] Z. Bouchal, J. Wagner, and M. Chlup, Opt. Commun. **151**, 207 (1998).
[7] P. Szwaykowski and J. Ojeda-Castaneda, Opt. Commun. **83**, 1 (1991).
[8] A. J. Cox and D. C. Dibble, J. Opt. Soc. Am. A **9**, 282 (1992).
[9] J. Rosen, B. Salik, and A. Yariv, J. Opt. Soc. Am. A **12**, 2446 (1995).
[10] J. A. Davis, E. Carcole, and D. M. Cottrell, Appl. Opt. **35**, 599 (1996).
[11] J. A. Davis, E. Carcole, and D. M. Cottrell, Appl. Opt. **35**, 2159 (1996).
[12] A. Vasara, J. Turunen, and A. T. Friberg, J. Opt. Soc. Am. A **6**, 1748 (1989).
[13] W.-X. Cong, N.-X. Chen, and B.-Y. Gu, J. Opt. Soc. Am. A **15**, 2362 (1999).
[14] E. M. Frins, J. A. Ferrari, A. Dubra, and D. Perciante, Opt. Lett. **25**, 284 (2000).
[15] A. Dubra and J. A. Ferrari, Am. J. Phys. **67**, 87 (1999).
[16] A. Papoulis, *Systems and Transforms with Applications in Optics* (McGraw-Hill, New York, 1968), pp. 235–239.
[17] M. Born and E. Wolf, *Principles of Optics*, 6th ed. (Pergamon Press, Oxford, 1980), Appendix III.
[18] M. Mansuripur, in *Handbook of Optics*, edited by M. Bass, 2nd ed. (McGraw-Hill, New York, 1995), Vol. 1, Chap. 31.